JOURNAL OF MATERIALS SCIENCE 25 (1990) 4541–4548

Fracture features of a silicon-dispersed aluminium alloy extruded from rapidly solidified powder

J. ZHOU, J. DUSZCZYK
Laboratory for Materials Science, Delft University of Technology, Rotterdamseweg 137, 2628 AL Delft, The Netherlands

The tensile fractography of an Al–20Si–3Cu–1Mg alloy consolidated from rapidly solidified powder by extrusion has been investigated using optical and electron microscopy, and related to the processing conditions as well as the tensile behaviour of the alloy at room and elevated temperatures. The alloy studied shows distinct fracture features owing to the presence of dispersed silicon crystal particles with a bimodal distribution in size and of prior powder particle boundaries in the extrudate. It has been found that at room temperature cracks initiate by cracking the primary silicon crystal particles. Crack propagation occurs along the interfaces between the eutectic silicon crystal particles and the matrix and also between the prior powder particles, where microvoids are formed by the interfacial decohesion. At 300° C, the fracture of the alloy involves microvoid nucleation, growth and coalescence at the interfaces between the silicon crystal particles and the aluminium matrix and between the prior powder particles. It has also been observed that the fractographic features of the alloy correspond well to the processing conditions including extrusion temperatures and subsequent heat treatment. The importance of minimizing the coarsening of the silicon crystals in processing in order to use the full strength potential of the alloy investigated is emphasized.

1. Introduction

Aluminium alloys with high silicon contents produced via the rapid solidification and powder metallurgy (RS-PM) route are regarded as a very important alloy system potentially for use in automobile, electric and aircraft industries [1–8]. One of the advantages that the rapid solidification brings about is the fine dispersion of silicon crystals in the aluminium matrix, thus providing the possibility of producing alloys for high-performance applications. In contrast, conventional ingot metallurgy generally gives rise to large silicon crystals which easily crack under low stresses, thus resulting in a premature failure of the material. Since the introduction of the rapid solidification technique to these alloys, a number of previous investigations have been focused on atomization and consolidation techniques [9, 10]. No effort, however, has been directed to the study of the fracture behaviour of the consolidated powder alloys.

In the RS-PM hypereutectic Al–Si alloys having undergone hot consolidation, there are two kinds of silicon crystal particles dispersed in the aluminium matrix, the primary and the eutectic. The primary silicon crystal particles are block-like with a size around 5 μm. The eutectic particles are massive in quantity and granular in shape with a size of about 1 μm. They form a so-called bimodal distribution of hard second-phase particles in a ductile matrix. The fracture mechanisms of these alloys are beyond the general description of fracture modes for common aluminium alloys. They mainly depend upon such metallurgical factors as: (1) the size and distribution of the silicon crystal particles, (2) the cohesion between the silicon crystal particles and the matrix, and (3) the ease with which the particles crack [11, 12]. Obviously, all these factors are related to the processing conditions of the alloys, most noticeably solidification rate, consolidation temperature and subsequent heat treatment. A further complicating factor in the fracture of the PM Al–Si alloys is added by the oxides which are present on prior powder particle boundaries (PPBs). These oxides are formed during atomization and subsequent handling in an oxidizing atmosphere, and fragmented during consolidation. The effect of the PPBs with the fragmented oxides on the mechanical properties and fracture behaviour of other PM Al alloys is controversial [13–18]. Clearly, the influence of the PPBs depends on oxidation degree, oxide properties, powder particle characteristics and processing conditions. Therefore, it is of particular importance to understand the fracture behaviour of the Al–Si alloys processed via the newly developed RS-PM route, which principally governs the mechanical properties and service life of the alloys.

The objective of the present work was to evaluate and characterize the fracture mechanisms of the PM silicon-dispersed aluminium alloys as a function of post-atomization processing conditions and service

0022–2461/90 $03.00 + .12

temperatures. Optical, scanning electron (SEM) and transmission electron (TEM) microscopy were used in the investigation.

2. Experimental procedure

2.1. Raw material

An Al–20Si–3Cu–1Mg alloy was chosen as a representative one in the silicon-dispersed aluminium alloy system for this study. The chemical composition of the alloy was 20% Si, 3.1% Cu, 1.3% Mg, 0.3% Fe(wt) and balance aluminium. The powder of the alloy was air atomized at a cooling rate of 10^4 to 10^6 K sec^{-1}. The morphology of the powder particles was, in the majority, tear-drop shaped. This shape is believed to be caused by the oxide film formed on the surfaces of atomized droplets [19]. The powder particle size varied from 5 to 150 μm with a median size of 20 to 30 μm, measured by means of image analysis (Joyce–Loeb). The microstructure of the atomized powder was very fine with the silicon-crystal sizes ranging between 1 and 8 μm. Auger electron spectroscopy revealed that the powder particles were covered by aluminium- and magnesium-rich oxides with an average depth of 40 to 43 nm [20].

2.2. Processing

The atomized powder was first cold compacted to a density of about 65% and degassed. Consolidation by hot extrusion was then performed at a reduction ratio of 20:1, at a ram speed of 5 mm sec^{-1} and at the temperatures between 325 and 475° C. In order to examine the effect of heat treatment subsequent to the extrusion on tensile and fracture behaviour, the as-extruded material was investigated and compared to the heat-treated, although the alloy is usually considered to belong to the heat-treatable aluminium alloy systems. A standard T6 temper treatment was applied to a part of the extrudate. The T6 temper involved a solution treatment at 470° C for 1.5 h followed by quenching in water, a natural ageing for 4 d and an artificial ageing at 120° C for 24 h.

2.3. Tensile tests

Specimens coaxial with the extrusion direction were machined. Their gauge length was 30 mm and diameter was 6 mm. The tests were conducted at both room and elevated temperatures on the specimens in the as-extruded and as-T6 tempered conditions, using a Tira test 2300 machine equipped with a microprocessor. The initial strain rate used was 5.6×10^{-3} sec^{-1}. For the elevated temperature tests, a split furnace was fitted on to the machine. Two thermocouples were placed in touch with the specimen necks. Before testing, the specimens were exposed to their testing temperatures (100, 200 and 300° C) for 100 h in order to evaluate their thermal stability.

2.4. Fractographic examination

Fracture surfaces were first examined visually, and then with optical and electron microscopy. Metallographic specimens were carefully prepared on the longitudinal sections of fracture surfaces, etched by a modified form of Keller and Wilcox's reagent (2% HCl–4% HNO_3–1% HF–H_2O). Observation was made on a Neophot-2 microscope. SEM specimens for the observation of fracture morphology were plated with gold to prevent charging of oxides, and a Jeol JXA 50A microscope was employed. For the identification of second phase, a Tracor (NS 880) X-ray energy dispersive system (EDS) attached to the SEM was used. TEM specimens were finally thinned with an ion mill. A Philips EM-400 microscope with energy dispersive analysis of X-ray (EDAX) was used to assist the investigation.

3. Results and discussion

3.1. Tensile tests

The results of tensile tests at room temperature and 300° C are summarized in Table I. For all the specimens in both the as-extruded and as-T6 tempered conditions, tested at and below 200° C, stress–strain curves did not exhibit a well-defined yield point. It is important to note that fracture at room temperature occurred suddenly while the material was work-hardening, before the attainment of a peak strength, as shown in Fig. 1. This indicates that the material failed prematurely before reaching its intrinsic strength. The elongation at fracture was very low, and no appreciable necking was observed. The fracture plane was perpendicular to the tensile direction. At 300° C, necking with a considerable percentage of plastic elongation prior to fracture occurred.

From Table I, it can be seen that in general both the 0.2% proof and ultimate tensile strengths varied with the extrusion temperature, being lower at a higher temperature. The reason for this is that a higher extrusion temperature brought about more coarsening of the dispersed silicon crystals as well as of the aluminium matrix microstructure. Particularly at the extrusion temperature of 475° C, the strength of the extrudate was reduced, because the adiabatic heating detrimentally coarsened microstructure. It is also noticeable

TABLE I Tensile-testing results of the PM alloy at room temperature and at 300° C

Extrusion temperature (° C)	Specimen state	UTS (MPa)		0.2% PS (MPa)		Elongation (%)	
		RT	300° C	RT	300° C	RT	300° C
325	extruded	369	140	288	126	2.8	20
350	extruded	354	122	265	110	3.7	22
400	extruded	360	140	262	120	3.9	21
450	extruded	322	105	237	96	3.9	30
475	extruded	310	102	249	95	1.7	18
325	tempered	401	101	328	96	3.4	17
400	tempered	430	106	321	98	3.7	18

RT = room temperature, UTS = ultimate tensile strength, 0.2% PS = 0.2% proof strength.

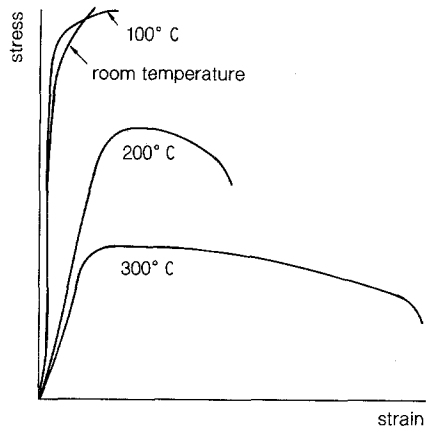

Figure 1 Stress–strain characteristics of the extruded alloy at different testing temperatures.

from Table I that the effect of the extrusion temperature on the tensile properties of the alloy was not as strong after the T6 temper as in the as-extruded state. This can be explained by the fact that the substructure in the aluminium matrix created during extrusion was eliminated by the heat treatment.

The strength of the material decreased with the testing temperature. The influence of the extrusion temperature on strength diminished with rising testing temperature, at 300° C in particular, where the balance between strain hardening and dynamic restoration dominantly governed the strength of the alloy. It is interesting to find that above 200° C the as-T6 tempered strength did not show any increase over the as-extruded; that on the contrary the latter was higher. The T6 temper has, nevertheless, been regarded as a normal treatment applied to the material. The finding implies that the necessity of employing the T6 temper for the material used at high temperatures is doubtful. The explanation of this result will be given later with the help of fractographic analysis.

3.2. Macrofractography

The alloy tested at and below 200° C, exhibited a topographical feature of a chevron pattern with a diverging point at the origin of fracture. The fracture origin was exclusively located at the edge of the specimens, irrespective of the extrusion temperatures and alloy state (as-extruded or as-T6 tempered). The fracture surfaces were flat and perpendicular to the tensile axis. This suggests that the fracture initiated at the origin and then propagated quickly along the chevron lines from one side of the specimen to the other. Macroscopically, the fracture appears to belong to a pure brittle pattern. For the specimens fractured at 300° C, the crack initiation site was not observable, and fracture surfaces were more ragged when compared to those at the lower temperatures. It implies that the fracture at this temperature may be classified as a ductile type.

3.3. Microfractography

3.3.1. At room temperature

The observation of the tensile fracture surfaces of the alloy in the as-extruded state and tested at room temperature revealed a peculiar morphology, which is difficult to classify according to the commonly-used definitions of fracture types. Figs 2a and b show the SEM fractographs taken at the origin of fracture from the alloy extruded at 325 and 450° C, respectively, by tracing back along the chevron lines on the fracture surfaces. It can be seen that there are some facets similar to cleavage in the region near the edge of the specimens. These are definitely the crack initiation sites. Obviously, this feature is different from that of other aluminium alloys, from which the cleavage-like appearance normally cannot be observed.

In the remaining part of the fracture surfaces there are extremely fine, shallow microvoids with a uniform size. It is found that the microvoids are associated with the small particles having a size of about 1 μm. Moreover, the centre-to-centre distance between two particles correlates well with that of two microvoids. Fig. 3 shows the TEM analysis with EDAX, indicating that the small particles are silicon-based with a certain amount of copper (referred to as the eutectic silicon crystal particles hereafter). The presence of the facet-like feature and the microvoids on the fracture surfaces indicates that both the conditions which favoured the occurrence of ductile and brittle fractures coexisted in the material.

SEM at low magnifications presents the important

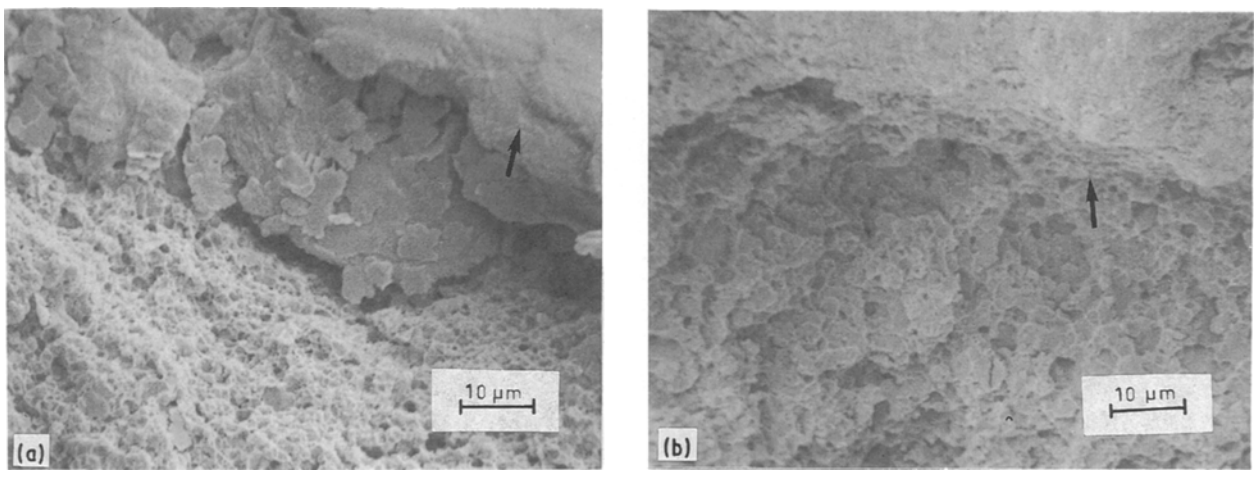

Figure 2 SEM fractographs taken at the fracture origin from the specimens extruded at (a) 325° C, and (b) 450° C, and tested at room temperature, showing a mixed fracture appearance.

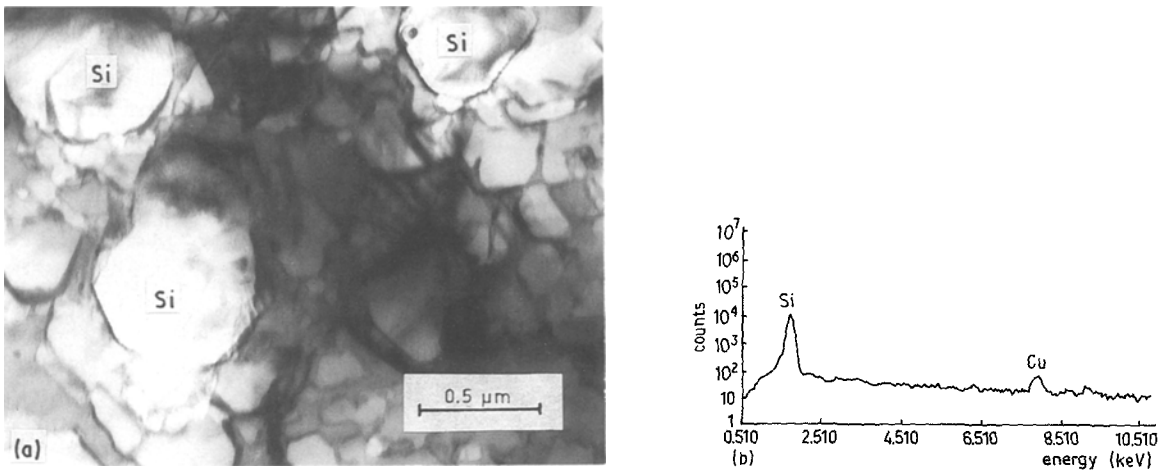

Figure 3 (a) TEM image and (b) EDAX spectrum of the small, eutectic silicon crystal particles.

information that in the vicinity of the fracture origin, there are depressed regions which correspond to the tips of the prior powder particles elongated during extrusion, as indicated by arrows in Fig. 4. This implies that a process of pulling apart of the prior powder particles could be involved in the fracture of the consolidated powder material. This phenomenon was also observed in other PM aluminium alloys [14, 16]. It can be easily understood that defects or inclusions like oxides, in spite of having been fragmented during extrusion, were situated on the PPBs. During the tensile test, locally inhomogeneous plastic flow of the aluminium matrix could arise around these oxides, resulting in stress concentrations. Debonding might then take place at some PPBs where the interparticle bonding was relatively weak, to relieve the concentrated stress. This facilitated the crack propagation along the debonded PPBs. It is therefore clear that debonding at the PPBs is partially responsible for the low elongation and early failure of the material.

Figs 5a and b show the optical fractographs of the material processed and tested under the same conditions as the above. It can be seen that microvoids are formed around the eutectic silicon-crystal particles, implying that no significant growth and coalescence took place before fracture. This evidence confirms that the eutectic silicon crystal particles with a high volume fraction caused the fracture surfaces with the "dimpled" appearance. On the optical fractographs (Fig. 5) the bimodal distribution of second-phase particles is clear. The cracking of the relatively large, block-like particles with an average size of 5 μm is visible (indicated by arrows), around which large voids are located. The identification of these particles was made by means of SEM with EDS (Fig. 6), revealing that the block-like particles are silicon-rich (referred to as the primary silicon crystal particles hereafter). The metallographic examination of an unbroken specimen showed that the cracking of these primary silicon crystal particles played an important role in the fracture process of the alloy. The concentrated stress at the primary particles reached such a high level that at a relatively low mean tensile stress local strain energy was sufficient for the generation of new crack surfaces.

The above evidence suggests the following fracture mechanisms successively operating in the PM material. Shortly after the occurrence of plastic flow during tensile testing, large stress concentrations are first generated at the relatively large, primary silicon crystal particles. As the massive, dispersed silicon crystal particles embedded in the aluminium matrix greatly restrict the mobility of dislocations, they prevent the relief of these stresses. The cracking of the primary

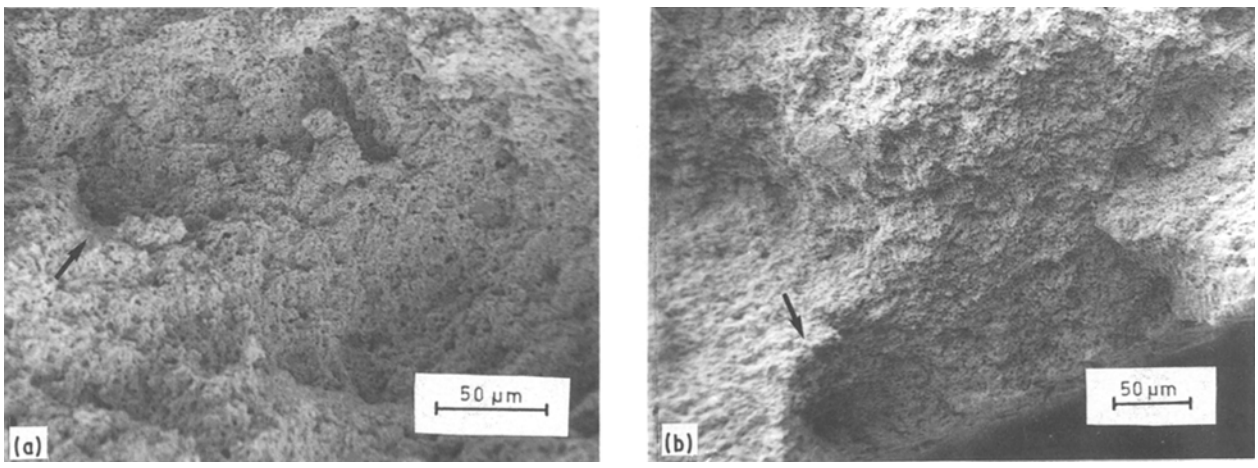

Figure 4 SEM fractographs at low magnifications, illustrating the depressed regions on the fracture surfaces, resulting from the debonding at the prior powder particle boundaries. Extrusion temperature: (a) 325° C and (b) 450° C.

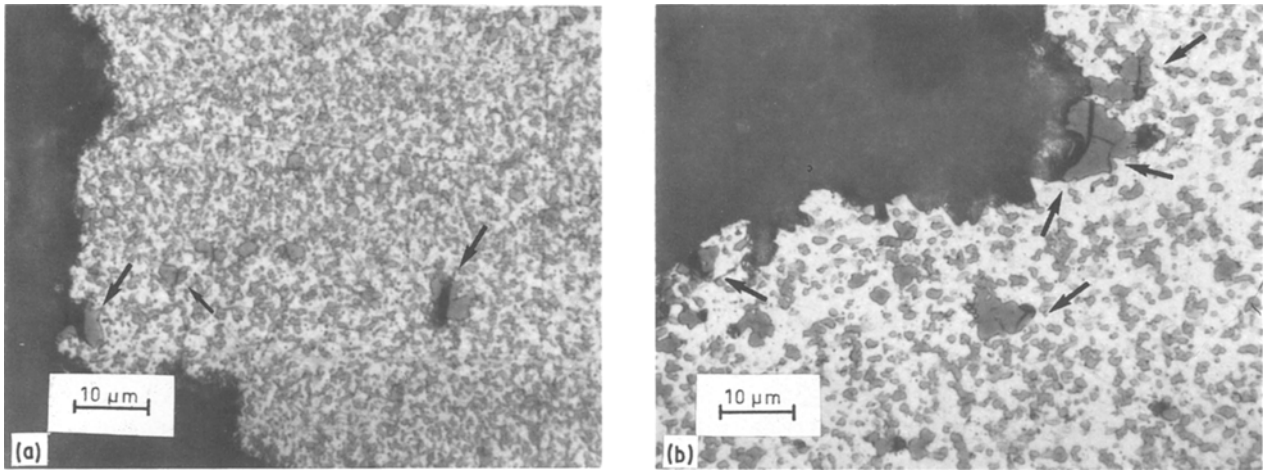

Figure 5 Optical fractographs on the longitudinal sections of the specimens extruded at (a) 325° C, and (b) 450° C, showing the cracked primary silicon crystal particles and the decohesion around the eutectic silicon crystal particles.

silicon crystal particles then occurs in a cleavage manner. But the crack tip is blunted by the eutectic silicon crystal particles, which prevents a further cleavage. With the increase of tensile stress, microvoids are initiated at the eutectic silicon crystal particles by interfacial decohesion. At the same time, because the concentration of oxides at the PPBs is higher than that in the interior, microvoids also nucleate at the PPBs. Upon the onset of a crack at a place close to the edge of the specimen, it quickly propagates by linking the cracked particles, the decohered interfaces and the debonded PPBs which are nearly coplanar. The mechanisms proposed above are schematically described in Fig. 7, which explains well the tensile behaviour of the PM alloy studied. Clearly, the cracking of the primary silicon crystal particles is a main cause for the curtailed ductility and strength of the material. Therefore, production and retention of fine primary silicon crystals in the whole processing route is of the utmost importance for obtaining a high strength with adequate ductility of the PM alloy.

Comparison of Figs 2 and 5 indicates that the size of microvoids is directly related to the silicon crystal size and density, and therefore to the cooling rate during powder production and extrusion temperature during consolidation. The microvoid size is basically controlled by the number of activation sites and required stress for the microvoid nucleation. It is known that the void nucleation occurs first at large particles in view of the accumulation of a critical dislocation density [21]. The stress, σ_c, required for void nucleation is proportional to the inverse square root of the particle size

$$\sigma_c = KR^{-1/2}$$

where K is a constant and R is the particle radius. Thus the silicon crystal particles with a smaller size are more resistant to decohesion with the aluminium matrix. The material with the smaller silicon crystal particles needs a higher tensile stress to initiate microvoids and therefore exhibits a higher strength. This result stresses the importance of preventing the growth of the silicon crystals during extrusion by using a relatively low extrusion temperature, provided that this is allowed by the power capacity of the extrusion press [22].

Figs 8a and b show the SEM fractographs of the T6-tempered material. The fracture surfaces are composed of numerous microvoids and a few large dimples which are associated with the primary silicon crystal particles. Apparently, the microvoid size in Fig. 8 is larger than that in Figs 2a and b. This was undoubtedly caused by the coarsening of the silicon crystals during the T6 temper. The enhanced strength of the T6-

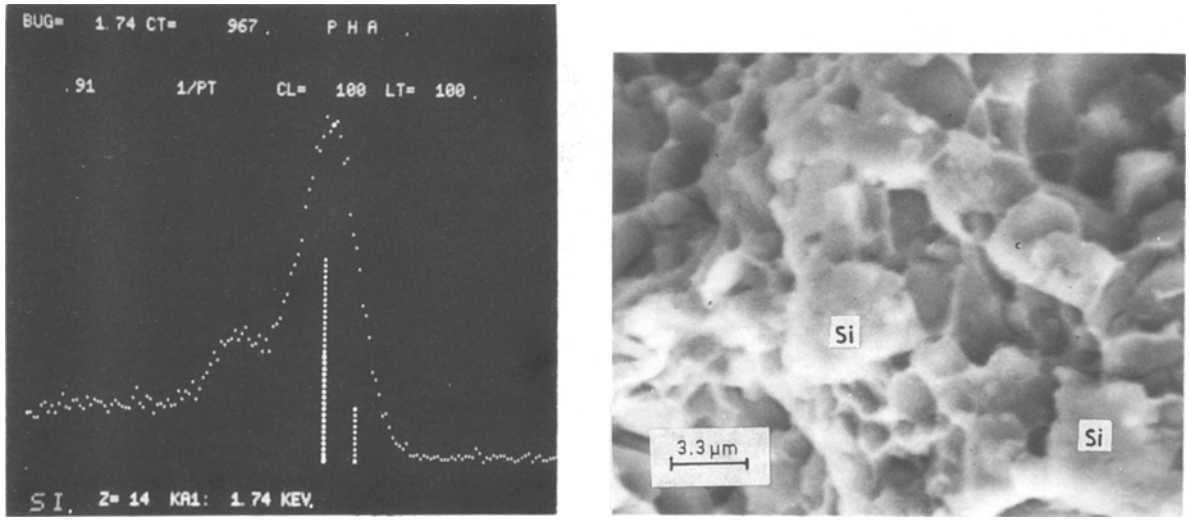

Figure 6 SEM fractograph with EDS spectrum of the aluminium matrix and the large, primary silicon crystal particles.

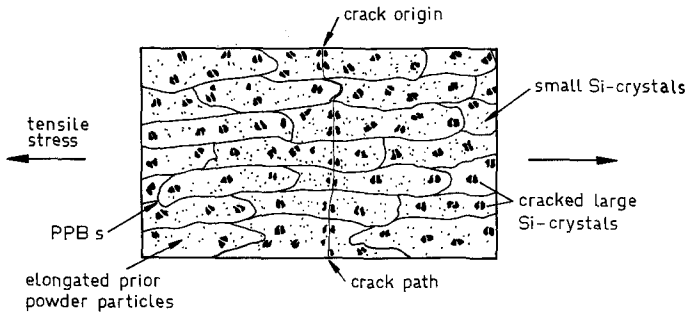

Figure 7 Schematic description of the fracture mechanisms for the PM silicon-dispersed aluminium alloy at room temperature.

tempered material at room temperature is attributed to the effect of precipitation hardening, which overcomes the negative effects of the silicon crystal growth and the matrix recrystallization occurring during heat treatment. A comparison of Figs 8a and b shows that the influence of the extrusion temperature on fracture morphology can still be observed from the difference in microvoid sizes, even though the heat treatment was performed afterwards. Debonding at the PPBs was occasionally observed, but the occurrence was less as compared with that in the as-extruded material. This implies that the interparticle bonding was improved to a certain extent by the T6 temper. According to the SEM fractographic observation and tensile behaviour, the fracture process of the T6-tempered material is basically the same as that of the extruded material in spite of the fact that the aluminium matrix was recrystallized and precipitation occurred. The optical fractography (Fig. 9) gives a clear confirmation of the fracture mechanisms proposed above. Many primary silicon crystals were cracked and large dimples are located around them, as indicated by arrows in Fig. 9. The cracked silicon crystal particles formed a discontinuous separation of the specimens on the transverse sections. The linkage of the cracked silicon crystals and debonded interfaces resulted in the final failure of the material.

3.3.2. At elevated temperatures

The fracture morphology of the specimens tested at 100 and 200° C is similar to that at room temperature, and thus the fracture mode cannot be expected to differ very much. The fracture at a higher temperature is of more interest. Fig. 10 shows the SEM fractographs of the extruded and T6-tempered material fractured at 300° C. In comparison with Figs 2 and 8, there is no significant difference in microvoid size, which implies that the exposure to this temperature for 100 h did not cause a great growth of the silicon crystals. The debonding at the PPBs at 300° C in a brittle manner is not evident, because in this case the material could yield by a process of thermally-activated dislocation cross-slip, before the stress reached a sufficient level to cause a direct separation along the PPBs. However, it is observed that large dimples are situated at the PPBs. This indicates that a process of microvoid initiation, growth and coalescence occurred at the PPBs during tensile testing. Figs 10a and c show the triple conjunction of the prior powder particles, which is clearly outlined by large dimples. This is direct evidence of the PPBs being involved in the fracture of Al–Si alloy at the high temperature.

It can also be seen from Fig. 10 that the dimples are generally larger and deeper, but not uniform in size. Optical fractography on the longitudinal section revealed a much lower occurrence of the primary silicon crystal cracking. Large dimples around the primary particles were found. It can be understood that at that temperature the material can adjust itself to accommodate the strain to some extent during tensile testing. Because the massive silicon crystal dispersion in the material greatly restricts the motion of dislocations, the decohesion between the relatively large, primary silicon crystal particles happens where the strain discontinuity is great enough to create new interfaces by decohesion. With a further increase of

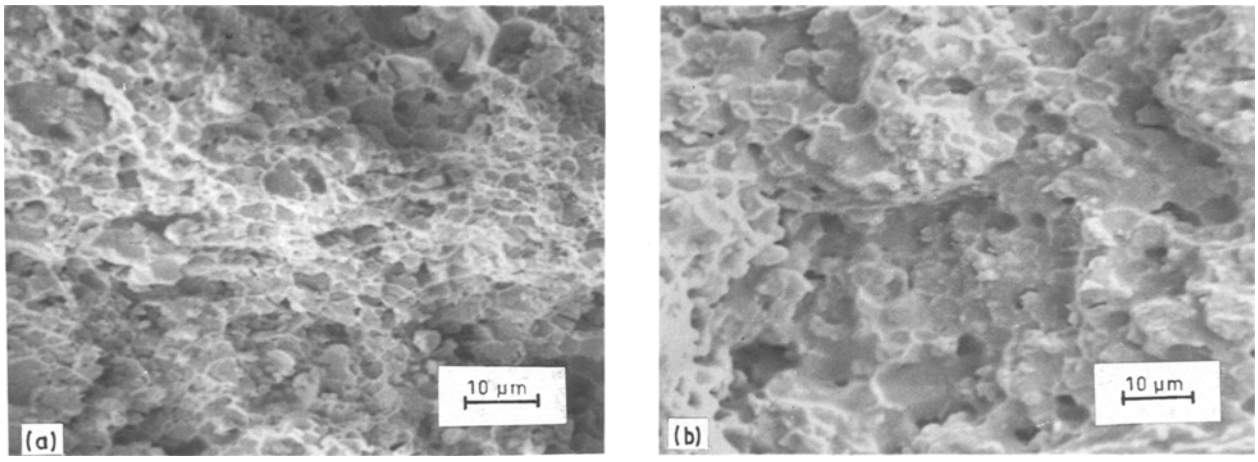

Figure 8 SEM fractographs of the T6-tempered specimens extruded at (a) 325° C, and (b) 450° C, showing the influence of extrusion temperature on the microvoid size of the heat-treated material, and the coarsened microvoids after the T6 temper.

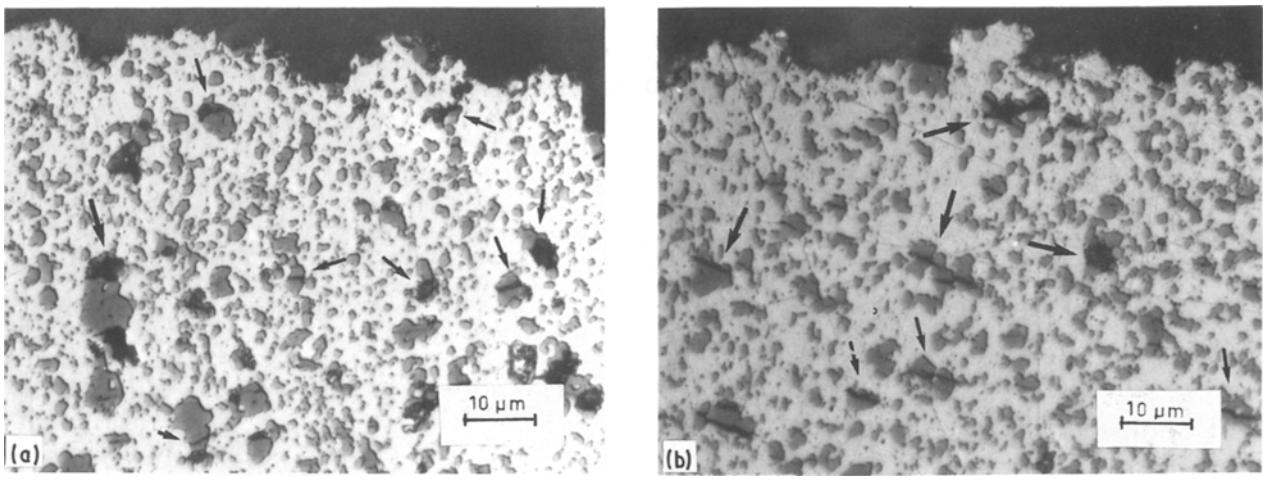

Figure 9 Optical fractographs of the T6-tempered specimens, showing the cracking of the primary silicon crystal particles and the decohesion at the interfaces between the eutectic silicon crystal particles and the matrix.

the tensile stress, the initiation of microvoids shifts to the smaller silicon crystal particles while the previously formed microvoids grow. Because silicon crystals are not continuous on the transverse sections, there is some space for the microvoids to grow and coalesce until the final linkage of the decohered interfaces. This gives rise to some ductility of the PM material at this temperature, as shown in Table I. Therefore, the material at 300° C principally shows a ductile type of fracture, although the decohesion between the silicon crystals and the aluminium matrix as well as at the PPBs is involved in the fracture process.

It can also be noted from Fig. 10 that the dimple size is greater for the material having experienced the T6 temper. As stated earlier, it is governed by the number of initiated microvoids and the latter is, in turn, related to the size of the silicon crystals. In the T6-tempered material, silicon crystal particles were coarsened during the solution treatment at 470° C,

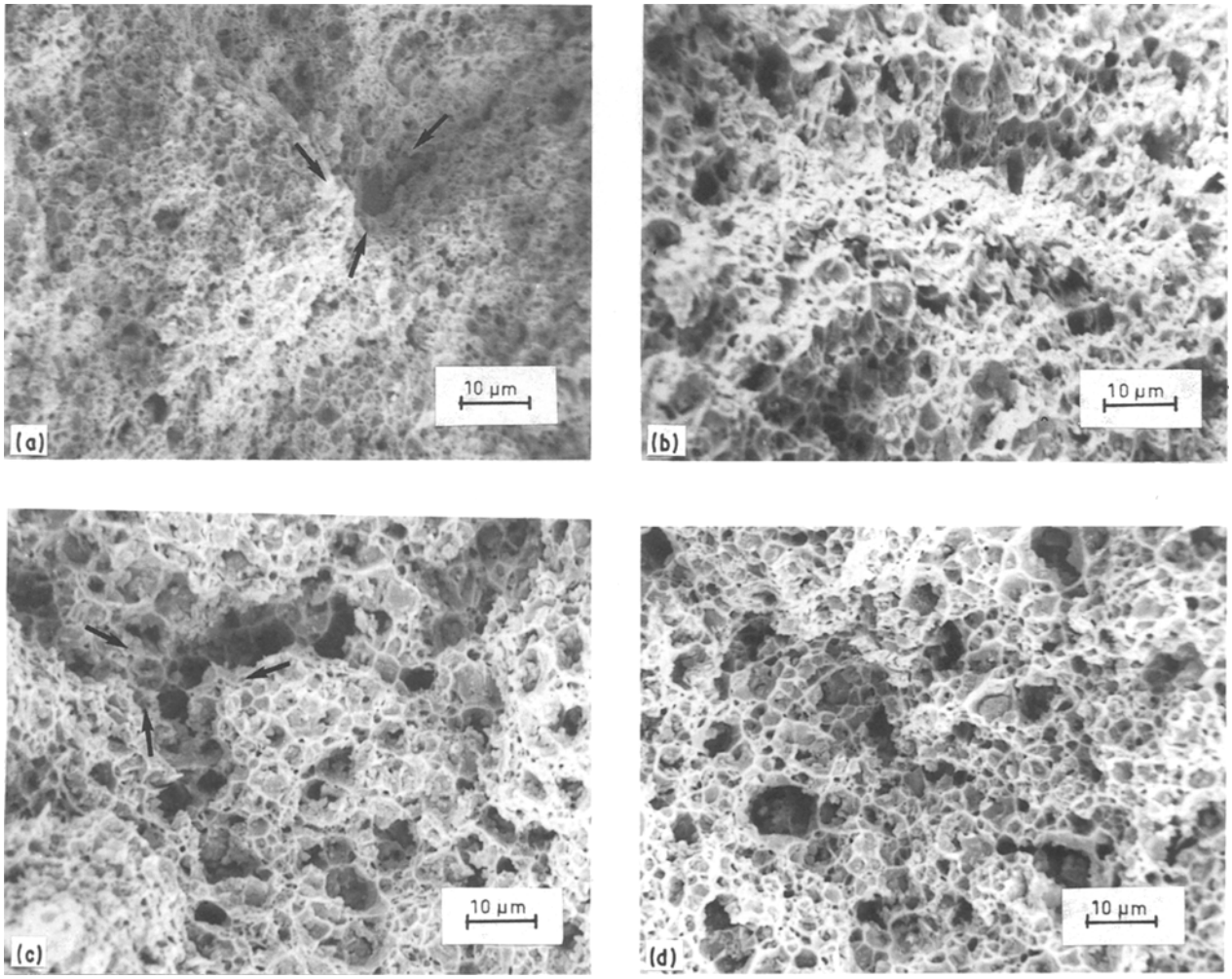

Figure 10 SEM fractographs of the specimens fractured at 300° C, (a) extruded at 325° C, (b) extruded at 450° C, (c) extruded at 325° C and T6-tempered, and (d) extruded at 400° C and T6-tempered.

and hence microvoids initiated at a lower stress. At 300° C, the effect of precipitation strengthening was diminished, the main strengthening mechanism being the silicon crystal dispersion. The T6-tempered material with coarsened silicon crystals, therefore, exhibits a lower strength than the extruded material. This accounts for the tensile properties at the elevated temperature as shown in Table I. The result suggests that for the material used at 300° C, the T6 temper can be eliminated as it brings about coarsening of the silicon crystal particles and thus early occurrence of microvoid initiation as well as final failure.

4. Conclusions

1. The silicon-dispersed aluminium alloy, produced via the powder metallurgy route, at room temperature shows a fracture mode different from that of common aluminium alloys. It fractures in a brittle manner, but very fine dimples appear on the fracture surface.

2. It is suggested that the fracture mechanisms of the PM silicon-dispersed aluminium alloy in the as-extruded and as-T6 tempered states, at and below 200° C, involve primary silicon crystal cracking and the decohesion between the eutectic silicon crystals and the aluminium matrix, as well as between the prior powder particles. The cracking of the primary silicon crystal particles is mainly responsible for the low ductility of the material.

3. The microvoid size on the fracture surface corresponds well to the silicon crystal size. The material with the finer silicon crystal particles obtained at a lower extrusion temperature thus exhibits a higher strength value. Retention of the fine silicon crystals in the extrusion process is of great importance to approach the intrinsic strength of the PM alloy.

4. The material at 300° C fractures in a ductile manner by microvoid nucleation, growth and coalescence at the interfaces between the silicon crystals and the matrix and at the prior powder particle boundaries.

5. The lower strength of the T6-tempered material at 300° C results from the coarsening of the silicon crystal particles occurring during the heat treatment. It is thus suggested that for the material used at this temperature, the T6 temper is not necessary.

Acknowledgements

The authors are indebted to Ing. E. J. A. van Dam for his assistance with SEM analysis and to Professor B. M. Korevaar for his support and stimulating discussion. Thanks are also due to the Showa Denko K. K., Chichibu, Japan, who supplied the atomized powder used in this work. The financial support of the Royal Academy of Science in the Netherlands (KNAW), the Foundation for Technological Research (STW) and the Foundation for Fundamental Research of Matter (FOM) is gratefully acknowledged.

References

1. C. F. DIXON and H. M. SKELLY, *Int. J. Powder Metall.* **4** (1965) 28.
2. H. M. SKELLY and C. F. DIXON, *ibid.* 7 (1971) 47.
3. T. HIRANO and T. FUJITA, *J. Jpn Inst. Light Metals* **37** (1987) 670.
4. T. FUJITA, F. KIYOTA, T. HIRANO and Y. KOJIMA, *ibid.* **37** (1987) 677.
5. K. SHIBUE and S. YAMAUCHI, *Sumitomo Light Metal Tech. Rep.* **27** (1986) 22.
6. T. HIRANO, F. OHMI, S. HORIE, F. KIYOTO and T. FUJITA, in Proceedings of the 1st International Conference on Rapidly Solidified Materials, San Diego, California, USA, February 1985, edited by P. W. Lee and R. S. Carbonara (ASM, Metals Park, Ohio, 1985) p. 327.
7. S. TSUCHIDA, *J. Jpn Inst. Light Metals* **37** (1987) 656.
8. N. KUROISHI, Y. ODANI and Y. TAKEDA, *Metal Powder Rep.* **40** (1985) 642.
9. J. DUSZCZYK and J. L. ESTRADA, in Proceedings of the Australian Bicentennial International Conference on Mechanical Engineering, "New Materials and Processes for Mechanical Design", Brisbane, Australia, May 1988 (Institution of Engineers, Australia, 1988) p. 96.
10. I. YAMANCHI, I. OHNAKA, S. KAWAMOTO and T. FUKUSAKO, *Trans. Jpn Inst. Metals* **27** (1986) 195.
11. G. T. HAHN and A. R. ROSENFIELD, *Metall. Trans.* **6A** (1975) 653.
12. R. H. VAN STONE and J. A. PSIODA, *ibid.* **6A** (1975) 668.
13. T. SHEPPARD and M. A. ZAIDI, *Metal Sci.* **18** (1984) 236.
14. YOUNG-WON KIM, W. M. GRIFFITH and F. H. FROES, *J. Metals* **37** (1985) 27.
15. F. J. GURNEY, D. J. ABSON and V. DEPIERRE, *Powder Metall.* **17** (1974) 46.
16. P. K. DOMALAVAGE, N. J. GRANT and Y. GEFEN, *Metall. Trans.* **14A** (1983) 1599.
17. E. K. IOANNIDIS, G. J. MARSHALL and T. SHEPPARD, *Mater. Sci. Technol.* **5** (1989) 56.
18. I. OHNAKA, I. YAMAUCHI, S. KAWAMOTO and T. FUKUSAKO, *J. Mater. Sci.* **20** (1985) 2148.
19. K. AKECHI, Y. ODANI and N. KUROISHI, *Sumitomo Electric Tech. Rev.* **24** (1985) 191.
20. J. L. ESTRADA and J. DUSZCZYK, *J. Mater. Sci.* **25** (1990) 886.
21. I. G. PALMER and G. C. SMITH, in "Oxide Dispersion Strengthening", Proceedings of a Symposium of the 2nd Bolton Landing Conference, Bolton Landing, New York, June 1966), edited by G. S. Ansell, T. D. Cooper and F. V. Lenel (Gordon and Breach, New York, 1968) p. 253.
22. J. DUSZCZYK, in Proceedings of the 8th International Light Metals Congress, Leoben-Vienna, Austria, June 1987, edited by F. Jeglitsch (Aluminium-Verlag, Dusseldorf, 1988) p. 760.

Received 8 May
and accepted 29 September 1989